

Tuning the oxidation of carbon monoxide using nanoassembled model catalysts

U. Heiz *, A. Sanchez, S. Abbet, W.-D. Schneider

Institut de Physique de la Matière Condensée, Université de Lausanne, CH-1015 Lausanne-Dorigny, Switzerland

Received 29 February 2000

Abstract

While the oxidation of CO has long been considered to be structure insensitive, nano-assembled model catalysts consisting of size-selected metal clusters (Au_n , Pt_n , Pd_n , and Rh_n , $n = 1\text{--}20$), supported on thin $\text{MgO}(1\ 0\ 0)$ films, reveal distinct size-effects. When adding a single Pt atom to Pt_{14} , platinum clusters increase their reactivity by a factor of three. Rh_{20} shows the highest reactivity of all the investigated clusters, oxidizing about 13 CO molecules per cluster at 350 K. While F-centers on MgO films transform Au_8 from an inert to an active catalyst, the reactivity of Pd_8 is not suppressed when deposited on defect-poor films. These different catalytic properties are rationalized within simple frontier orbital models, whereas for Au_8 the reaction mechanism for the low temperature oxidation of CO is elucidated within first-principle calculations. © 2000 Elsevier Science B.V. All rights reserved.

1. Introduction

Boudard defines a structure sensitive reaction as a catalytic process depending on size and morphology of the catalytically active compound [1]. For example, the cyclotrimerization of acetylene is catalyzed with highest efficiency on $\text{Pd}(1\ 1\ 1)$ facets [2–9] and reveals distinct differences on small Pd_n ($n = 1\text{--}30$) clusters [10]. A structure insensitive reaction, e.g., the oxidation of carbon monoxide has long been considered as such [11], depends neither on size nor shape of the involved particles [1]. To study different catalytic processes in detail, the concept of model catalysts was introduced by Poppa [12]. Such model catalysts consist of metal

particles supported on well-characterized oxide surfaces. In most case studies performed so far, the active metal particles are composed of hundreds or thousands of atoms [11,13]. In this size range, the number of electronic states is large and the electronic structure of the particles is well described by electronic bands. This is the reason why intrinsic bulk properties of a given element do not change as function of the precise particle size. As a consequence, the observed structure sensitivities and insensitivities are surface effects, and they are dependent on the electronic surface properties and surface morphologies like densities of kinks, steps as well as the types of crystalline facets the particle's surface is composed of [14]. For example, the $\text{Ag}(1\ 1\ 1)$ surface supports an occupied surface state as opposed to $\text{Ag}(1\ 0\ 0)$; such differences are one possible reason responsible for structure sensitivities in catalytic reactions [15]. Likewise, for $\text{Ni}(1\ 1\ 1)$ the work function, or in the language of

* Corresponding author. Tel.: +41-21-692-36-67/53; fax: +41-21-692-36-35.

E-mail address: heiz@dpmail.epfl.ch (U. Heiz).

molecular orbital theory, the position of the highest occupied molecular orbital (HOMO) is 5.35 eV, whereas for Ni(110), it is only 5.04 eV [16], illustrating the different electronic surface properties and the concomitant changing chemical properties of different crystal planes. Finally, the lattice constants of various crystal planes differ. This structural parameter determines whether a molecular overlayer involved in a catalytic reaction is adsorbed in a commensurate or incommensurate configuration and whether there is activation of the molecules due to deformation. Furthermore, considering the large active metal particle as a sphere with radius R , the surface-to-bulk ratio is changing monotonically with $1/R$ and thus, the catalytic properties vary accordingly. Superimposed to this monotonic change of the chemical reactivity of large particles is their size-dependent behavior solely characterized by the particles' morphology, e.g. the density of steps or kinks [17–19].

For small clusters, however, these simple concepts fail. In nano-scale clusters, the valence electrons are highly confined and quantum effects become dominant. Therefore, each cluster with a specific number of atoms has its own intrinsic chemical and physical properties [20–27] and new concepts have to be developed to classify size-dependent catalytic properties of nano-scale clusters. A possible starting point for this classification is using the large body of data obtained from gas phase cluster studies. In the early eighties, clusters of the monovalent atom sodium were first produced by the group of Schumacher [28] driven by his knowledge of the important role of small silver particles in the photographic process and by the group of Knight [20]. Striking discontinuities in the mass spectra at magic numbers of 8, 20, 34, 40, ... (Na atoms per cluster) were discovered. The Berkeley group [20] achieved a fundamental understanding of these abundance spectra within the Jellium model [20,29–31], well known to nuclear physicists. In this way, the electronic shell structure of metallic clusters was established. In analogy to the classic periodic table of the elements used to predict chemical and physical properties, a periodic table for clusters can be constructed simply by filling the electronic shells representing

the different periods [32]. In this way, we find monovalent clusters, such as Na_3 , Na_9 , and Na_{19} analogous to the alkaline metals or the open-shell clusters Na_7 and Na_{17} similar to halides. These clusters might reveal changing reactivities like the corresponding elements. This simple comparison suggests, therefore, that for small clusters, where the electronic structure is dominant in changing the cluster's properties, a new and exciting chemistry is waiting for to be discovered. Such a size-dependent variation of the chemical properties was observed in several gas phase studies, where reactivities of small metal clusters were investigated. Bérces et al. measured absolute rate coefficients for the reaction of Nb_n clusters ($n = 2–20$) with H_2 and N_2 at different temperatures [33], confirming the low reactivities of Nb_8 , Nb_{10} , and Nb_{16} measured in earlier experiments [34,35]. They recognized an anticorrelation of the reactivity with an effective ionization potential of the cluster that includes the polarization of the charge on the cluster cation. This correlation between the electronic structure and the reactivities of niobium clusters was also observed experimentally by Kietzmann et al. [36]. These authors estimated the HOMO–LUMO gap from photoelectron spectra and observed closed shells and a large HOMO–LUMO gap for the unreactive cluster sizes. In addition, Bérces et al. clearly observed biexponential kinetic plots, indicative of the presence of different isomers with distinct reactivities. They suggested that in addition to electronic, steric effects also play a decisive role in determining cluster reactivities [33]. Shi et al. and Hagen et al. even investigated a whole catalytic cycle and studied the catalytic oxidation of CO on free platinum and gold clusters in a molecular beam experiment [37,38].

In this work, we went a step towards real catalysts and investigated the oxidation of CO on size-selected supported clusters of Au_n , Pt_n , Pd_n , and Rh_n ($1 \leq n \leq 20$) and discovered a strong size-dependent behavior. The aim of this work is to highlight some important examples in the oxidation of CO on cluster catalysts. In most cases, due to the lack of accurate simulations at the present time, we rationalize our results with simple models. First, the observed size-dependency for the CO-oxidation within an element is compared with

the evolution of the electronic structure and the morphology as function of cluster size. The different reactivities of a single cluster size (Au_{13} , Pt_{13} , Pd_{13} , and Rh_{13}) are then compared and rationalized with the different electronic structure of these hypothetically ‘geometrically closed shell’ clusters [39]. Finally, we review results of first-principle calculations [40,41], which revealed the complete reaction mechanisms of the oxidation of CO on deposited Au_8 .

2. Experimental

The used model catalysts, consisting of size-selected metal clusters on thin $\text{MgO}(1\ 0\ 0)$ films are prepared by recently developed cluster-deposition facilities [42]. Briefly, the clusters are formed by a high frequency laser evaporation source (Fig. 1). The produced singly charged clusters (Au_n^+ , Pt_n^+ , Pd_n^+ , Rh_n^+) are transported by ion optics through differentially pumped vacuum chambers, deflected by 90° by a quadrupole deflector and mass selected

by a quadrupole mass filter with a mass limit of 4000 amu. A typical mass spectrum of Rh_n clusters, where the expansion conditions were optimized for the production of small clusters [42], is shown in Fig. 2. The monodispersed cluster beam is deposited with low kinetic energy ($E_{\text{kin}} < 0.2$ eV per atom [42]) onto thin $\text{MgO}(1\ 0\ 0)$ films at 90 K under ultrahigh vacuum (UHV) conditions (10^{-10} Torr). The total energy of the deposition process consists of the kinetic energy, the involved chemical binding energy between the Au_n^+ , Pt_n^+ , Pd_n^+ , and Rh_n^+ clusters and the MgO surface (0.4–1.4 eV per interacting atom [40,43,44]), the neutralization energy, as well as a negligible Coulomb interaction of the incoming cluster ion and its induced polarization charge and image charge on the oxide film surface and the metal surface, respectively. Consequently, as the kinetic energies of the impinging clusters correspond to soft-landing conditions ($E_{\text{kin}} \leq 1$ eV per atom) [45–47], and as the total energy gained upon deposition is at least a factor of two smaller than the binding energies of the investigated clusters ranging from 2 to 5 eV

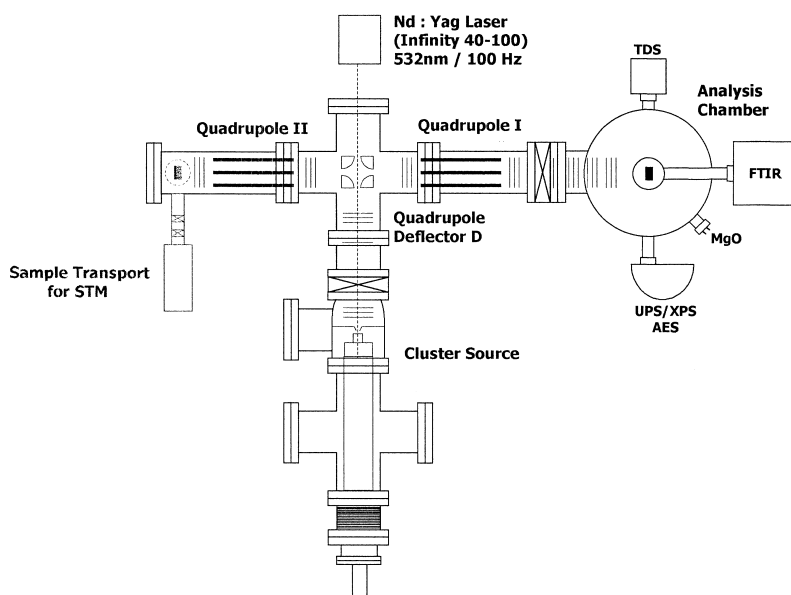


Fig. 1. Experimental setup composed of high frequency laser evaporation cluster ion source driven by a 100 Hz Nd:Yag laser (Coherent Infinity 40/100), ion optics with a quadrupole deflector and quadrupole mass spectrometer and the analysis chamber. The latter is equipped with a mass spectrometer for thermal desorption spectroscopy (TDS), a Fourier transform infrared (FTIR) spectrometer, a spherical electron energy analyzer used for Auger electron spectroscopy (AES), a gas-handling system equipped with a calibrated molecular beam doser, and evaporation sources for thin oxide film preparations.

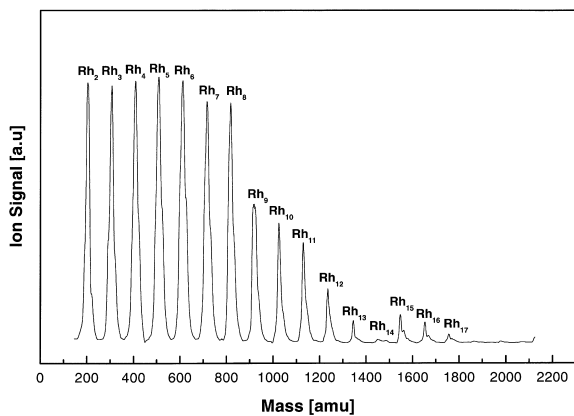


Fig. 2. Mass spectrum of Rh_n clusters. The cluster source (He pressure, laser delay) and the transmission of the ion optics are optimized for obtaining maximal signal for Rh_5 .

[48–53], fragmentation of the cluster is excluded. Soft-landing of the clusters is confirmed in an independent experiment, where small nickel clusters (Ni , Ni_2 , and Ni_3) are deposited under the same conditions and saturated with CO [54]. It could be shown that only nickel carbonyls with the nucle-

arity of the deposited clusters are formed. In the experiments presented in this work, between 0.14% and 0.40% of a monolayer of size-selected clusters ($1 \text{ ML} = 2.2 \times 10^{15} \text{ clusters/cm}^2$) are deposited at 90 K, in order to land them isolated on the surface and to prevent agglomeration of the clusters on the support [55].

The $MgO(100)$ films are prepared in situ for each experiment by epitaxially growing the oxide films on a $Mo(100)$ surface by evaporating magnesium at 300 K in a $^{16}O_2$ background [56]. These films show similar properties as the bulk analog as evidenced with LEED, EELS, and XPS (Fig. 3(a)–(c)), however, a reproducible density of defects is present on the surface [40]. These defects are titrated with small molecules like CO or NO (Fig. 3(d)/(e)). In this work, we distinguish between defect-rich and defect-poor MgO films. The defect-poor films are characterized by desorption of CO at 120 K (Fig. 3(d)), which results from adsorption of CO on domain boundaries most probably. Defect-rich films are characterized by additional desorption of about 1% monolayer (ML) of NO at 650 K (Fig. 3(e)), which is believed to originate

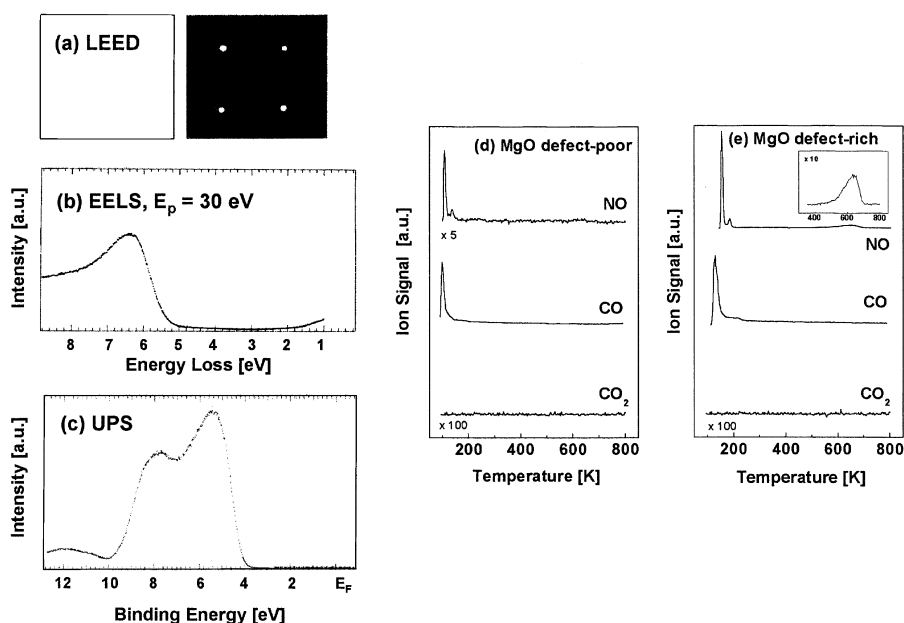


Fig. 3. Characterization of the $MgO(100)$ thin films: defect-poor films (see text) show (a) LEED, (b) EELS, and (c) XPS spectra typical for $MgO(100)$ bulk systems. However, CO desorbs at an untypically high temperature of 120 K (d). Defect-rich films are characterized by the desorption of NO at around 600 K (e).

from NO adsorbed on F-centers [40,57]. Both oxide films have been proven to be inert towards the oxidation of CO, e.g., no CO₂ is produced with the experimental conditions used for the cluster experiments. For the study of the catalytic activity of the clusters, the model catalysts are first exposed by a molecular beam doser to an average of 20 ¹⁸O₂ molecules per deposited atom at a sample temperature of 90 K, and subsequently to the same number of ¹³CO or ¹²CO molecules. This is crucial, as it is well known from single crystal studies that the initial amount of oxygen and CO on the surface and the ratio of these molecules during oxidation may influence the reactivity [58–61]. In a temperature programmed reaction (TPR) experiment, the products of the chemical reaction are monitored by mass spectrometry. The reactivities obtained in this one-heating-cycle process are defined as the produced number of ¹³C¹⁸O¹⁶O or ¹²C¹⁸O¹⁶O molecules per cluster. This catalytic action is determined by integrating the TPR signal of the CO₂ molecules and normalizing to the number of deposited clusters. For this procedure, the mass spectrometer has been calibrated using the known amount of desorbing CO from a Mo(1 0 0) single crystal [62] and taking account of the different detection sensitivities for CO and CO₂. The number of deposited clusters is obtained by integrating the measured ion current on the substrate over the deposition time.

3. Results

Fig. 4 shows the TPR spectra for the CO-combustion on supported Au_{*n*}, Pt_{*n*}, Pd_{*n*}, and Rh_{*n*} (*n* = 8, 13, 20) clusters. Surprisingly, each cluster size shows a different reactivity and reaction temperature, although the oxidation of CO has long been considered as structure insensitive. As for the bulk analogs, gold clusters reveal the lowest reactivity, expressed in the number of ¹³C¹⁸O¹⁶O formed per cluster. Interestingly, for gold clusters Au₈ is the most reactive cluster (1.1 ± 0.1 CO₂) at the lowest temperatures (140 and 240 K) when deposited on defect-rich films, whereas for Au₂₀ (1.9 ± 0.1 CO₂), in addition to the oxidation of CO at 140 K, CO₂ is mainly formed at high tempera-

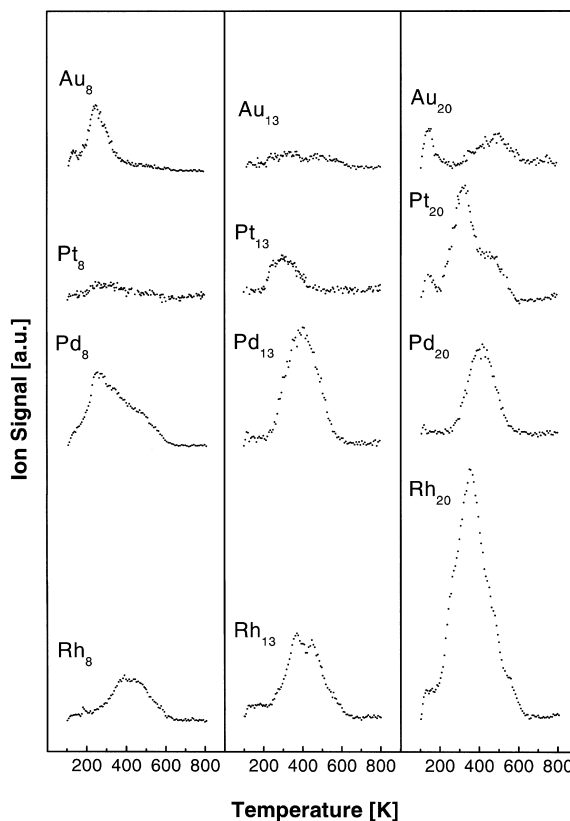


Fig. 4. CO combustion on Au_{*n*}, Pt_{*n*}, Pd_{*n*}, and Rh_{*n*} (*n* = 8, 13, 20) obtained by a one-heating-cycle experiment. The model catalysts were first exposed to an average of 20 molecules of ¹⁸O₂ per deposited metal atom and subsequently by the same number of carbon monoxide. The CO₂ signal was scaled to the coverage of the deposited metal clusters.

ture (500 K). In contrast to these electronically closed shell clusters, Au₁₃, reveals the lowest reactivity. Such a strong size-dependency is also observed for Pt_{*n*}, where the number of formed CO₂ per cluster increases by a factor of 9 when going from Pt₈ (0.6 ± 0.1 CO₂) to Pt₂₀ (5.6 ± 0.1 CO₂) (Fig. 4). In addition, Pt₂₀ reveals two high temperature mechanisms at around 350 and 500 K, where for the octamer CO₂ is produced only at 300 K. It is interesting to note that only the larger clusters (Pt_{*n*}, *n* > 14) form CO₂ at a temperature of 140 K [27]. For the other two metals, palladium and rhodium, even the octamers show considerable reactivity for the oxidation of CO (3.0 ± 0.1 and 2.8 ± 0.1 molecules of CO₂ per Pd₈ and Rh₈,

respectively). Of all the investigated clusters, Rh_{20} is by far the most reactive one ($12.7 \pm 0.1 \text{ CO}_2$). The interaction of CO with the octamers of the different elements was investigated by FTIR. Fig. 5 reveals the different vibrational frequencies of ^{13}CO adsorbed on Au_8 (2055 cm^{-1}), Pt_8 (2020 cm^{-1}), Pd_8 ($2037, 2014, 1893 \text{ cm}^{-1}$) and Rh_8 (2020 cm^{-1}) measured at 90 K. All spectra show dominant frequencies typical for CO adsorbed in an on-top configuration, only the spectrum of Pd_8 reveals frequencies typical for bridge bonded CO (1893 cm^{-1}). In the case of Au_8 , the observed ^{13}CO frequency is the closest to the one of gas phase ^{13}CO (2096 cm^{-1}), and therefore, CO is the weakest

bound to this cluster. Note the relatively broad adsorption bands for Pd_8 and Rh_8 , indicative for several COs bond to the cluster surface. It is informative to compare the reactivities of clusters with the same nuclearity. Here, we concentrate on Au_{13} , Pt_{13} , Pd_{13} , and Rh_{13} , in order to reveal the influence of the different electronic structures on their chemical properties. Au_{13} shows by far the lowest reactivity ($0.6 \pm 0.1 \text{ CO}_2$), followed by Pt_{13} ($1.9 \pm 0.1 \text{ CO}_2$). The highest reactivities in this series are observed for Pd_{13} ($4.2 \pm 0.1 \text{ CO}_2$) as well as Rh_{13} ($4.4 \pm 0.1 \text{ CO}_2$).

For Pt_{20} , Fig. 6 shows desorption of catalytically produced CO_2 and CO, which is not oxidized

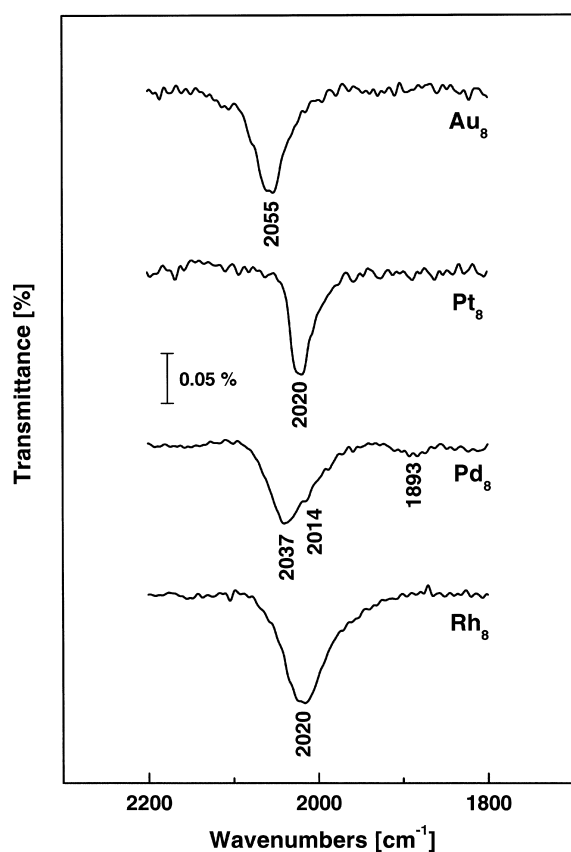


Fig. 5. Shown are infrared absorption frequencies of ^{13}CO adsorbed on (a) Au_8 , (b) Pt_8 , (c) Pd_8 , and (d) Rh_8 . All spectra are taken at 90 K. Note the high frequency of CO adsorbed on the gold octamer. Note that the frequency for ^{12}CO can be calculated by using $\nu(^{13}\text{CO})/\nu(^{12}\text{CO}) = (\mu(^{12}\text{CO})/\mu(^{13}\text{CO}))^{1/2}$, with μ being the reduced mass.

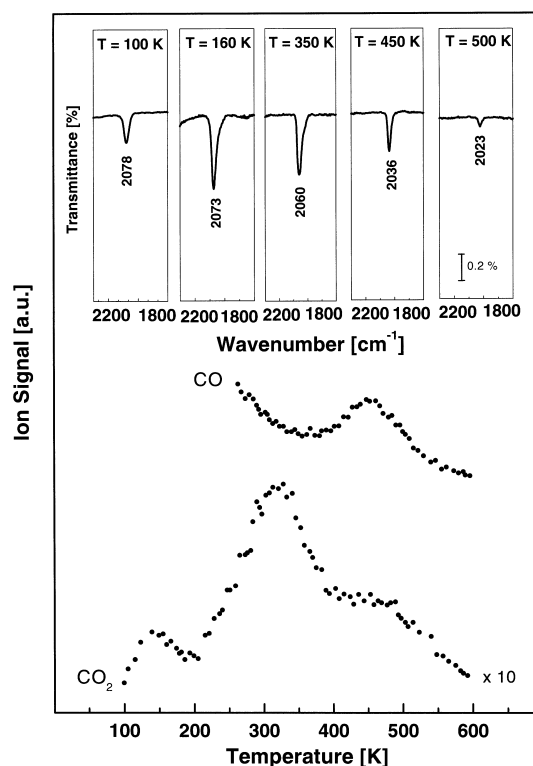


Fig. 6. Temperature programmed reaction: CO_2 production and CO desorption for Pt_{20} as a function of temperature, (\cdots) data. Isotopically labeled $^{12}\text{C}^{16}\text{O}$ and $^{18}\text{O}_2$ are used to unambiguously attribute the catalytic activity to the supported clusters. The number of desorbing molecules can be estimated by integrating the TPR spectra (see text). Inset: FTIR spectra of adsorbed CO during the catalytic oxidation (e.g. coadsorbed with O_2) are shown. The samples are annealed to the indicated temperatures and all spectra are then recorded at 90 K.

by the cluster. Note that the TPD for CO is only depicted from 200 to 600 K. The low temperature range is characterized by the well-known CO desorption typical for these thin MgO-films [63]. In comparison, the evolution of the IR absorption of CO during the reaction reveals an increase in the integrated absorption intensity between 100 and 160 K. From 160 to 500 K, a distinct decrease of the integrated absorption intensity is observed, which is in concert with the oxidation of CO from 160 to 350 K, whereas between 350 and 550 K the desorption of CO also contributes to the decrease of the IR signal. Note that there is no evidence of adsorbed CO₂ as inferred from the missing IR absorption in the CO₂ frequency range.

Finally, the influence of the defect density on the MgO(100) thin films was investigated for the oxidation of CO on Au₈ and Pd₈. Au₈ is only reactive when deposited on defect-rich films (Fig. 7), whereas for Pd₈ the reactivity expressed in the number of oxidized CO does not reveal such a drastic change when varying the defect density on the MgO films (Fig. 7).

4. Discussion

4.1. CO oxidation and its size-dependent evolution with cluster size

For the oxidation on the cluster surface to take place, several conditions have to be fulfilled. In an Eley–Rideal type of mechanism one of the reactant, in this case the O₂ molecule, has to be adsorbed on the catalyst. The activation of the molecule has to be such that the activation energy for the formation of the product is low enough that collisions with the incoming CO lead to the formation of CO₂. In a Langmuir–Hinshelwood type of reaction, both reactants are adsorbed on the surface and the activation energy for the CO₂ formation has to be lower than the desorption energies of the products. In addition, none of the reactants ought to block the reactive sites on the cluster. The one cycle heating experiments presented here are only sensitive to the Langmuir–Hinshelwood type of reaction.

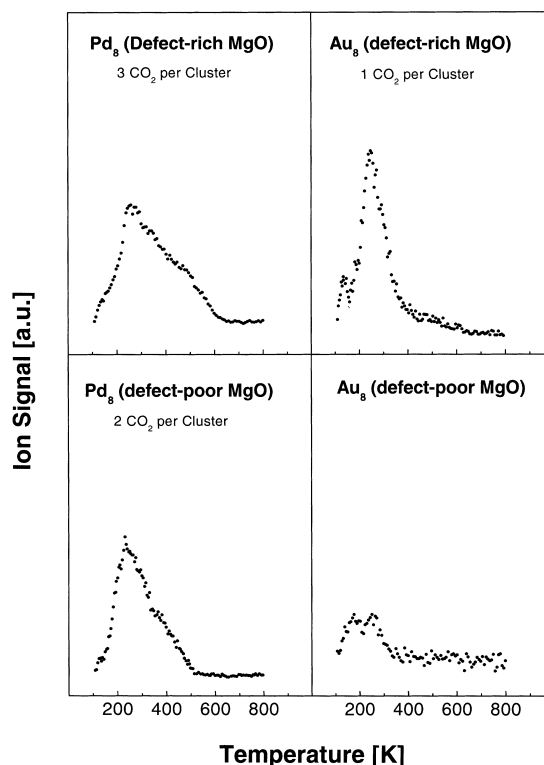


Fig. 7. CO combustion on Au₈ and Pd₈ deposited on defect-rich and defect-poor MgO films. Note the decrease in reactivity of Au₈ at 240 K when deposited on defect-poor films. For Pd₈ only the reactivity at higher temperature is suppressed on defect-poor MgO films.

Our results showed that such small clusters are already catalytically active and revealed element specific and size-dependent reactivities. As only CO₂ molecules with one isotopically labeled ¹⁸O atom are detected, the adsorbed oxygen is dissociated prior or during the oxidation of CO and no disproportionation reaction (¹³C¹⁶O + ¹³C¹⁶O → ¹³C¹⁶O₂) occurs. In most cases, the reaction is not stoichiometric as shown by CO desorbing during the reaction (shown for Pt₂₀ in Fig. 6). As expected, the reaction heat of the oxidation process is responsible for the immediate desorption of CO₂ from the cluster. This is inferred experimentally from the absence of IR absorptions at frequencies typical of adsorbed CO₂, and more directly from a comparison of the evolution of the vibrational frequencies of CO and the formation

of CO₂ and desorption of CO during the TPR experiment. The distinct increase in integrated absorption intensity between 100 and 160 K can be explained by migration of physisorbed CO to the cluster and/or reorientation of the adsorbed CO molecules and a concomitant enhanced absorption cross section.¹ At higher temperature, however, the decrease is in concert with the oxidation of CO, where between 350 and 550 K desorption of CO contributes to the changing signal. Very interestingly, Pt_n, Pd_n, and Rh_n are more prone to poisoning by carbon monoxide than Au_n clusters. In fact, only gold clusters revealed an unchanged CO combustion when first exposing to CO and then to O₂ in these one-heating-cycle experiments. This is related to the bond strength of CO to the clusters. The stronger the interaction with CO, the more likely the reactive sites are blocked as observed for Pt_n, Pd_n, and Rh_n. That this interaction is indeed the weakest for gold is shown by infrared spectroscopy wherein the highest absorption frequency of CO is observed for Au₈. The low adsorption energy of CO on gold is also confirmed by TPD experiments, which show that CO desorbs already at about 180 K in comparison to, e.g., 450 K for Pt₈.

In many cases, the dissociation of oxygen constitutes the first step in an oxidation reaction [58,60,64]. Thus, in order to understand to a first approximation, the size-dependent reactivity of each element, the knowledge of the evolution of the intrinsic cluster properties with size and its influence on the molecular or dissociative adsorption of oxygen on the cluster's surface are crucial. To first order, the interaction of oxygen with surfaces can be rationalized within the Newns–Anderson model [65,66]. In this model, the interaction of an adsorbate species with a small group of atoms of an extended surface is described within bonding and anti-bonding levels, reminiscent of the simple valence theory of diatomic molecules. The discrete adsorbate states couple with a con-

tinuum of states of the metal surface. This coupling with, e.g., the broad sp-bands of the metal results in broadened adsorbate levels due to the reduced lifetime of the electrons in the discrete adsorbate states. The resulting interaction is characterized as a weak chemisorption. The coupling of the adsorbate states with the narrower d-bands of the metal results in bonding and antibonding states; this interaction is called strong chemisorption. If we replace the molecule–surface interaction with the molecule–cluster interaction, the following size-dependent scenario emerges. For the oxygen molecule, the electronic states of interest are the bonding, fully occupied π_u and σ_g and the antibonding, half-occupied π_g^* orbitals. Providing there exists a resonance (energetically and symmetrically) between one of these orbitals and the cluster's density of state (DOS), adsorption and dissociation of O₂ is possible [67]. As shown by density functional theory (DFT) calculations, the d-band position is the most decisive parameter, when describing molecule–surface bonding [68]. Dissociation or activation of the adsorbed O₂ occurs when there is enough backdonation from the cluster into the antibonding π_g^* state or a sufficient donation from the π_u or σ_g into the cluster [69]. Both processes reduce the bond order of oxygen. If we apply this simple argumentation to the observations of the reactivity of deposited Pt_n clusters, the energy of the HOMO for different cluster sizes, associated with the energy of the center of the d-band, can be tuned from –9.0 eV, the ionization potential (IP) of the atom, to –5.32 eV, the Fermi energy of bulk platinum. Now, the increase in the catalytic activity from Pt₈ to Pt₂₀ can be correlated with the decrease of the IP and the change in the position of the center of d-band with increasing cluster size and the concomitant enhanced resonance with the antibonding π_g^* state of O₂. The maximum reactivity for Pt₁₅ [27] suggests that the resulting backdonation is largest for this cluster. Increasing the cluster size further, lowers the cluster's HOMO even more and may result in a weaker resonance with the antibonding π_g^* state of O₂, as the HOMO's energy passes the energy of this antibonding state. For the very small clusters, this backdonation is small as the energy mismatch of cluster's HOMO and π_g^* is large.

¹ IR in reflection mode is only sensitive to dynamical dipole moments perpendicular to the surface. Therefore using integrated absorption intensities to estimate CO concentrations on the surface have to be taken with care.

In this simple model, the interaction with the substrate is completely neglected. As shown by theoretical investigations, one of the major roles of the cluster–surface interaction is the charging of the clusters [40]. Therefore for cluster catalysts, where the reactivity is similar for different cluster charge states, this simplification may be valid to a first approximation for rationalizing trends in the size-dependent reactivities at least when structural changes of the clusters are small upon deposition. Gas phase studies indeed indicate that the charge-state of the clusters does not often alter the general trends in the size-dependent chemistry, if the clusters are composed of transition metals with partially filled d-states [70]. On the other hand, we show below that this interaction completely determines the reactivity of small gold clusters in the way that charge flows from the substrate to the cluster [40]. This is in line with gas phase studies where it was shown that only negatively charged clusters are reactive towards O_2 adsorption.

4.2. CO-combustion on the tridecamers: influence of the geometric and electronic structure

A comparison of the reactivities of the 13-atom clusters is elucidating as they are considered to have geometrically closed shell structures. For Pt_{13} , Pd_{13} [51], and Au_{13} [50],² the structures with cuboctahedral symmetry are predicted to be slightly more stable than the icosahedral structures. In contrast, for Rh_{13} , an icosahedral ground-state structure is calculated [71]. The average coordination number for the icosahedral structure is 6.5, whereas the cuboctahedral structure reveals a coordination number of 5.5 [50].² This suggests the low-coordinated clusters (Au_{13} , Pt_{13} , and Pd_{13}) to be more reactive when assuming that the structures of the clusters are only slightly perturbed by the interaction with the $MgO(100)$ film [40]. Such a trend, however, is not supported by the presented results. Therefore, purely geometrical arguments

² Very recent DFT-GGA calculations [39] indicate, however, that both neutral and anionic Au_{13} clusters prefer strongly deformed low-symmetry structures with an average coordination number per atom of about 5.1.

and the local morphology, which are often used for solid surfaces, not seem to be sufficient to explain these differences.

The observed chemical properties are, thus, mainly influenced by the varying electronic structures of the four molecular clusters. Calculations have shown that their electronic structure can be viewed as a superposition of atomic d-states and an electronic shell structure, characterized by the number of atomic s electrons in the cluster [51] (Fig. 8). For the noble metal cluster Au_{13} each atom contributes one delocalized valence electron and a closed d-shell. In this case, the HOMO is characterized by a discrete electronic shell state (Fig. 8). For Pd_{13} and Pt_{13} with an atomic $4d^{10}$ and $5d^96s^1$ configuration, respectively, the character of the electronic states around the Fermi level drastically changes (Fig. 8). For these clusters, the electronic states at the Fermi level are characterized by the superposition of atomic d-states. For Pd_{13} , an additional unoccupied shell- $2p^*$ state is situated just at the Fermi level [51]. This difference in the electronic structure is reflected in the chemical behavior of Au_{13} , Pd_{13} , and Pt_{13} in the following manner. In order to oxidize CO molecules efficiently at high temperature, several oxygen molecules have to be activated sufficiently upon adsorption. This occurs when there is enough hybridization between the antibonding π_g^*

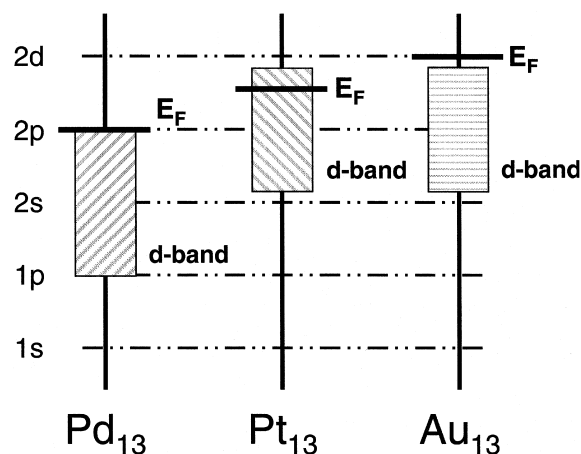


Fig. 8. The schematic energy level diagram for Pd_{13} , Pt_{13} , and Au_{13} [51].

state of oxygen and the cluster's electronic states at the Fermi level. Thus, the electronic states of oxygen hybridize more efficiently with the high density of d-states of palladium and platinum clusters. For Au_{13} , the bonding between the discrete shell states and the molecular electronic states of oxygen is, however, less likely. In fact, ab initio calculations showed that the HOMO and LUMO of Au_{13} are energetically below the antibonding state of oxygen; and therefore, no charge transfer from the cluster to the oxygen molecule is possible [72].

4.3. Cluster-support interaction: the role of defects

The gold octamer is only reactive when deposited on defect-rich $\text{MgO}(100)$ films. These defects are characterized experimentally and theoretically by the adsorption properties of NO and are identified with oxygen vacancies, F-centers (FC) [40,72]. The role of these defects is threefold [40]: first, the enhanced binding (5.56 eV) of Au_8 clusters to the $\text{MgO}(\text{FC})$ surface anchors them and thus, reduces their propensity for agglomeration and sintering, second, a charge transfer of 0.5 e to the gold cluster enhances the adsorption of oxygen and third the activation energy for forming CO_2 on the cluster is reduced. This finding is in accordance with early experiments of molecular oxygen adsorption on free gas-phase clusters showing that only even numbered *anionic* clusters react with gaseous O_2 molecules. The reaction mechanisms, occurring at 140 and at 240 K have been elucidated by extensive ab initio simulations [40]. First, these calculations describe the adsorbed Au_8 cluster as a deformed piece of a hexagonal closed-packed crystal with stacked five (bottom)- and three (top)-atom layers. The deposited gold octamer adsorbs both O_2 and CO molecules. In the optimized adsorption configuration, CO binds on top of a Au atom of the upper triangular facet of the deposited Au_8 . On the other hand, the O_2 molecule readily adsorbs at several sites, both on the upper Au_8 facet and at the interface between the adsorbed gold cluster and the underlying magnesia surface. In both cases, the adsorbed oxygen molecule is found to be activated to a peroxo O_2^* molecular state. For the oxidation of CO at 140 K, two possible reaction mechanisms were

proposed. In a first direct Eley–Rideal reaction mechanism, a CO molecule brought from the gas phase to the vicinity of the peroxo molecule on the top-facet of the gold cluster reacts spontaneously forming a CO_2 molecule weakly bound to the catalyst (~ 0.2 eV). Another reaction mechanism, which contributes to the low-temperature oxidation of CO is of the Langmuir–Hinshelwood type, where the two reactants are initially coadsorbed on the top-facet of the Au_8 cluster. A weakly adsorbed CO_2 molecule is formed after overcoming a small activation barrier of 0.1 eV. The oxidation of CO at 240 K is attributed to a reaction mechanism, where the peroxo O_2^* molecule bonded to the periphery of the interfacial layer of the cluster is involved. In the case where the gold octamer is bound to an FC, an activation energy of ~ 0.5 eV is found. Interestingly, this activation barrier significantly increases (~ 0.8 eV) when the cluster is bound to defect-free magnesia, which explains the experimental observation that the octamer is not reactive when deposited on defect-free magnesia. It is interesting to note that the reactivity of Pd_8 is not suppressed upon deposition on defect-poor $\text{MgO}(100)$ films, but only decreases at high temperature (500 K). These differences may again be explained by the different electronic structure of the two octamers. Charge transfer to the Pd_8 may have less effect, as the density of states around the Fermi level is characterized by the superposition of atomic d-states, in addition Pd clusters are already reactive as neutral species; therefore, subtle changes in their electronic structure upon deposition are less important than they are for Au_8 .

5. Conclusions

We have shown that the oxidation of CO is dependent on the size of small gold, platinum, palladium and rhodium clusters and on their distinct interaction with the oxide support. For gold clusters, it was found that the combustion of CO at low temperature (~ 240 K) on Au_8 is activated after deposition on defect sites of the MgO substrate. Interestingly, for Pd_8 the combustion of CO is not suppressed when adsorbed on defect-poor films. The geometrically closed shell clusters Pt_{13} ,

Pd₁₃, and Rh₁₃ as well as Au₁₃ all show a different reactivity, suggesting that their electronic structure mainly govern their reactivity. Au₁₃ shows a low density of states around the Fermi energy and a coupling with the antibonding state of oxygen is prevented. On the other hand for Pt₁₃ and Pd₁₃, the atomic d-states overlap the Fermi-level, resulting in a high density of states, and therefore these clusters become more reactive. In general, the evolution of the reactivities with cluster size correlate with the position of the atomic d-states with respect to the antibonding π_g^* O₂ state. These examples clearly show that the chemical properties of small metal cluster can be tuned as function of size and of the distinct cluster-support interaction.

Acknowledgements

We thank H. Häkkinen and U. Landman for stimulating discussions, critical reading of the manuscript and for communicating unpublished results. This work was supported by the Swiss National Science Foundation. U.H. thanks the Alexander v. Humboldt Stiftung for a fellowship.

References

- [1] M. Boudard, Adv. Catal. 20 (1969) 153.
- [2] W.T. Tysoe, G.L. Nyberg, R.M. Lambert, J. Chem. Soc. Chem. Commun. (1983) 623–625.
- [3] W.S. Sesselmann, B. Woratschek, G. Ertl, J. Kuppers, H. Haberland, Surf. Sci. 130 (1983) 245.
- [4] P.M. Holmblad, D.R. Rainer, D.W. Goodman, J. Phys. Chem. B 101 (1997) 8883–8886.
- [5] T.M. Gentle, E.L. Muetterties, J. Phys. Chem. 87 (1983) 2469–2472.
- [6] T.G. Rucker, M.A. Logan, T.M. Gentle, E.L. Muetterties, G.A. Somorjai, J. Phys. Chem. 90 (1986) 2703–2708.
- [7] H. Hoffmann, F. Zaera, R.M. Ormerod, R.M. Lambert, J.M. Yao, D.K. Saldin, L.P. Wang, D.W. Bennett, W.T. Tysoe, Surf. Sci. 268 (1992) 1–10.
- [8] R.M. Ormerod, R.M. Lambert, J. Phys. Chem. 96 (1992) 8111–8116.
- [9] G. Pacchioni, R.M. Lambert, Surf. Sci. 304 (1994) 208–222.
- [10] S. Abbet, A. Sanchez, U. Heiz, W.-D. Schneider, A.M. Ferrari, G. Pacchioni, N. Rösch, Surf. Sci. 454–456 (2000) 984–989.
- [11] C.R. Henry, Surf. Sci. Rep. 31 (1998) 231–326.
- [12] H. Poppa, Catal. Rev. Sci. Engng. 35 (1993) 359–398.
- [13] H.J. Freund, Angew. Chem. Int. Ed. Engl. 36 (1997) 452–475.
- [14] S. Dahl, A. Logadottir, R.C. Egeberg, J.H. Larsen, I. Chorkendorff, E. Toernqvist, J.K. Nørskov, Phys. Rev. Lett. 83 (1999) 1814–1817.
- [15] E. Bertel, P. Roos, J. Lehmann, Phys. Rev. B 52 (1995) R14 384–R14 387.
- [16] C. Kittel, in: R. Oldenbourg (Ed.), Einführung in die Festkörperphysik, vol. 7. Verlag, Muenchen, 1988.
- [17] L. Piccolo, C. Becker, C.R. Henry, J. E. Phys. D. 9 (1999) 415–419.
- [18] M. Frank, S. Andersson, J. Libuda, S. Stempel, A. Sandell, B. Brena, A. Giertz, P.A. Brühwiler, M. Bäumer, N. Martensson, H.-J. Freund, Chem. Phys. Lett. 279 (1997) 92–99.
- [19] D.W. Goodman, P.M. Holmblad, D.R. Rainer, J. Phys. Chem. B 101 (1997) 8883–8886.
- [20] W.D. Knight, K. Clemenger, W. de Heer, W.A. Saunders, M.Y. Chou, M.L. Cohen, Phys. Rev. Lett. 52 (1984) 2141.
- [21] R.L. Whetten, D.M. Cox, D.J. Trevor, A. Kaldor, Phys. Rev. Lett. 54 (1985) 1494.
- [22] I.M.L. Billas, A. Châtelain, W.A. deHeer, Science 265 (1994) 1682.
- [23] U. Heiz, A. Vayloyan, E. Schumacher, C. Yerezian, M. Stener, P. Gisdakis, N. Rösch, J. Chem. Phys. 105 (1996) 5574–5585.
- [24] A.P. Alivisatos, Science 271 (1996) 933–937.
- [25] T. Leisner, C. Rosche, S. Wolf, F. Granzer, L. Wöste, Surf. Rev. Lett. 3 (1996) 1105–1108.
- [26] U. Heiz, F. Vanolli, A. Sanchez, W.-D. Schneider, J. Am. Chem. Soc. 120 (1998) 9668–9671.
- [27] U. Heiz, A. Sanchez, S. Abbet, W.-D. Schneider, J. Am. Chem. Soc. 121 (1999) 3214–3217.
- [28] M.M. Kappes, R.W. Kunz, E. Schumacher, Chem. Phys. Lett. 91 (1982) 413–418.
- [29] W.A. deHeer, Rev. Mod. Phys. 65 (1993) 611–676.
- [30] W. Ekardt, Phys. Rev. B 29 (1984) 1558–1564.
- [31] K. Clemenger, Phys. Rev. B 32 (1985) 1359–1362.
- [32] U. Heiz, W.-D. Schneider, Physical chemistry of supported clusters, in: K.-H. Meiwes-Broer (Ed.), Metal Clusters at Surfaces – Structure, Quantum Properties, Physical Chemistry, Springer, Berlin, 2000, pp. 237–273.
- [33] A. Berces, P.A. Hackett, L. Lian, S.A. Mitchell, D.M. Rayner, J. Chem. Phys. 108 (1998) 5476–5490.
- [34] M.D. Morse, M.E. Geusic, J.R. Heath, R.E. Smalley, J. Chem. Phys. 83 (1985) 2293.
- [35] M.R. Zakin, R.O. Brickman, D.M. Cox, A. Kaldor, J. Chem. Phys. 88 (1988) 3555.
- [36] H. Kietzmann, J. Morenzin, P.S. Bechthold, G. Ganteför, W. Eberhardt, J. Chem. Phys. 109 (1998) 2275–2278.
- [37] Y. Shi, K.M. Ervin, J. Chem. Phys. 108 (1998) 1757–1760.
- [38] J. Hagen, L. Souciou, T. Bernhard, T. Leisner, U. Heiz, L. Wöste, submitted for publication.
- [39] H. Häkkinen, U. Landman, Phys. Rev. B 62 (2000) R2287–R2290.

- [40] A. Sanchez, S. Abbet, U. Heiz, W.-D. Schneider, H. Häkkinen, R.N. Barnett, U. Landman, *J. Phys. Chem. A* 103 (1999) 9573–9578.
- [41] H. Häkkinen, R.N. Barnett, U. Landman, *Phys. Rev. Lett.* 82 (1999) 3264.
- [42] U. Heiz, F. Vanolli, L. Trento, W.-D. Schneider, *Rev. Sci. Instrum.* 68 (1997) 1986.
- [43] I. Yudanov, G. Pacchioni, K. Neyman, N. Rösch, *J. Phys. Chem.* 101 (1997) 2786–2792.
- [44] I.V. Yudanov, S. Vent, K. Neyman, G. Pacchioni, N. Rösch, *Chem. Phys. Lett.* 275 (1997) 245–252.
- [45] K. Bromann, C. Felix, H. Brune, W. Harbich, R. Monot, J. Buttet, K. Kern, *Science* 274 (1996) 956–958.
- [46] H.-P. Cheng, U. Landman, *J. Phys. Chem.* 98 (1994) 3527.
- [47] W. Harbich, in: K.-H. Meiwes-Broer (Ed.), *Collision of Clusters with Surfaces: Deposition, Surface Modification and Scattering*, Springer, Heidelberg, 1999.
- [48] G. Valerio, H. Toulhoat, *J. Phys. Chem.* 100 (1996) 10828–10830.
- [49] S. Krueger, S. Vent, N. Rösch, *Ber. Bunsenges. Phys. Chem.* 101 (1997) 1640.
- [50] O.D. Haberlen, S.C. Chung, M. Stener, N. Rösch, *J. Chem. Phys.* 106 (1997) 5189–5201.
- [51] N. Watari, S. Ohnishi, *Phys. Rev. B* 58 (1998) 1665–1677.
- [52] S.H. Yang, D.A. Drabold, J.B. Adams, P. Ordejon, K. Glassford, *J. Phys.: Cond. Matter* 9 (1997) L39–L45.
- [53] A. Sachdev, R.I. Masri, J.B. Adams, *Z. Phys. D. Atoms Mol. Clusters* 26 (1993) 310–312.
- [54] U. Heiz, *Appl. Phys. A* 67 (1998) 621–626.
- [55] M.-H. Schaffner, F. Patthey, W.-D. Schneider, *Surf. Sci.* 417 (1998) 159.
- [56] M.C. Wu, J.S. Corneille, C.A. Estrada, J.-W. He, D.W. Goodman, *Chem. Phys. Lett.* 182 (5) (1991) 472.
- [57] U. Heiz, W.-D. Schneider, *J. Phys. D Appl. Phys.* 33 (2000) R85–R102.
- [58] J. Xu, J.T. Yates, *J. Chem. Phys.* 99 (1993) 725–732.
- [59] K.-H. Allers, H. Pfnür, P. Feulner, D. Menzel, *J. Chem. Phys.* 100 (1994) 3985–3998.
- [60] A. Szabo, M.A. Henderson, J.T. Yates, *J. Chem. Phys.* 96 (1992) 6191–6201.
- [61] A. Rar, T. Matsushima, *Surf. Sci.* 318 (1994) 89–96.
- [62] F. Zaera, E. Kollin, J.L. Gland, *Chem. Phys. Lett.* 121 (4/5) (1985) 464.
- [63] J.-W. He, A.E. Cesar, J.S. Corneille, M.-C. Wu, D.W. Goodman, *Surf. Sci.* 261 (1992) 167–170.
- [64] J.A. Rodriguez, D.W. Goodman, *Surf. Sci. Rep.* 14 (1991) 1.
- [65] D.M. Newns, *Phys. Rev.* 178 (1969) 1123.
- [66] P.W. Anderson, *Phys. Rev.* 124 (1961) 41.
- [67] A.W.E. Chen, R. Hoffmann, W. Ho, *Langmuir* 8 (1992) 1111–1119.
- [68] B. Hammer, O.H. Nielsen, J.K. Nørskov, *Catal. Lett.* 46 (1997) 31–35.
- [69] R. Hoffman, *Solids and Surfaces: A Chemist's View of Bonding in Extended Structures*, VCH Verlagsgesellschaft, GmbH: Weinheim, 1988.
- [70] M.R. Zakin, R.O. Brickman, D.M. Cox, A. Kaldor, *J. Chem. Phys.* 88 (1988) 5943.
- [71] B.V. Reddy, S.K. Nayak, S.N. Khanna, B.K. Rao, P. Jena, *Phys. Rev. B* 59 (1999) 5214–5222.
- [72] H. Häkkinen, R.N. Barnett, U. Landman, A. Sanchez, S. Abbet, U. Heiz, W.-D. Schneider, submitted for publication.